A new method of resolving annual precipitation for the past millennia from Tibetan ice cores

Wangbin Zhang[1], Shugui Hou[1,2,3], Shuang-Ye Wu[4], Hongxi Pang[1,2], Sharon B. Sneed[5], Elena V. Korotkikh[5], Paul A. Mayewski[5], Theo M. Jenk[6,7], and Margit Schwikowski[6,7]

[1]School of Geography and Ocean Science, Nanjing University, Nanjing 210023, China.

[2]Collaborative Innovation Center of Climate Change, Jiangsu Province, Nanjing, China.

[3]School of Oceanography, Shanghai Jiao Tong University, Shanghai 200240, China.

[4]Department of Geology and Environmental Geosciences, University of Dayton, Dayton, OH 45469, USA.

[5]Climate Change Institute, University of Maine, Orono, ME 04469, USA.

[6]Laboratory of Environmental Chemistry, Paul Scherrer Institute, CH-5232 Villigen PSI, Switzerland.

[7]Oeschger Centre for Climate Change Research, University of Bern, Sidlerstrasse 5, CH-3012 Bern, Switzerland.

Correspondence to: Shugui Hou (shugui@nju.edu.cn; shuguihou@sjtu.edu.cn)

Abstract. Net accumulation records derived from ice cores provide the most direct measurement of past precipitation. However, quantitative reconstruction of accumulation for past millennia remains challenging due to the difficulty in identifying annual layers in the deeper sections of ice cores. In this study, we propose a new method to quantify annual accumulation from alpine ice cores for past millennia, using as an example an ice core drilled at the Chongce ice cap in the northwestern Tibetan Plateau (TP). First, we used the Laser Ablation Inductively Coupled Plasma Mass Spectrometry (LA-ICP-MS) technology to develop an ultra-high-resolution trace element records in three sections of the ice core and identified annual layers in each section based on seasonality of these elements. Second, based on nine ^{14}C ages determined for this ice core, we applied a two-parameter flow model to established the thinning parameter of this ice core. Finally, we converted the thickness of annual layers in the three sample sections to past accumulation rates based on the thinning parameter derived from the ice-flow model. Our results show that the mean annual accumulation rates for the three sample sections are 109 mm/year

删除了: 2

(2511-2541 a B.P.), 74 mm/year (1682-1697 a B.P.) and 68 mm/year (781-789 a B.P.), respectively. For comparison, the Holocene mean precipitation is 103 mm/year. This method has the potential to reconstruct continuous high-resolution precipitation records covering millennia or even longer time periods.

删除了: 6

删除了: 84

1 Introduction

Precipitation, including both snowfall and rainfall, is a crucial component of the Earth's energy and water cycles, and is a variable parameter associated with atmospheric circulation in weather and climate studies (Kidd and Huffman, 2011). Accurate and reliable knowledge of precipitation is of paramount importance not only for the study of water resource management, but also for understanding and monitoring the Earth's climate change (Kidd and Huffman, 2011; Sun et al., 2018). The earliest systematic instrumental observations of precipitation (i.e., rain gauges) began in the eighteenth century in Europe, but they were not put in place until much later in other parts of the world (Sun et al., 2018). Our knowledge of precipitation in earlier times therefore relies on precipitation-sensitive proxy records from different types of biological and geological archives, e.g., tree rings, stalagmite, terrestrial and marine sediment, and ice cores (Cai et al., 2012; Kaspari et al., 2008; Thompson et al., 2006; Xu et al., 2019; Yang et al., 2014).

删除了: the most important and

删除了: Christiansen and Ljungqvist, 2017

Net accumulation recorded in alpine ice cores provides the most direct measurement for past precipitation, as glaciers are formed by accumulating annual layers of snow (Paterson and Waddington, 1984). However, in order to derive accurate net accumulation records, sampling resolution must be high enough to obtain reliable layer thickness information for the relevant timescale (typically annual, but may be centennial for low temporal resolution sites). In addition, the nonlinear thinning of annual layers caused by ice flow must be suitably constrained (Bolzan, 1985; Henderson et al., 2006; Roberts et al., 2015). The most common approach is to obtain annual-layer thickness based on the seasonal cycles of ice core parameters such as stable isotope ratio of oxygen in the water ($\delta^{18}O$), the concentration of major ions (e.g. Ca^{2+}, Mg^{2+}, NH_4^+, SO_4^{2-}), and the presence of melt layers (Thompson et al., 2018). The thinning parameter of ice cores is usually derived from an ice flow model constrained by the ages of absolute chronological markers, e.g., peak of beta and/or tritium activity from thermonuclear bomb testing in the second half of the 20th century, well-defined aerosol layers and/or tephra from large volcanic eruptions,

删除了: annual-

and radioactive dating method based on ^{210}Pb activity decay (Uglietti et al., 2016; Zhang et al., 2015). Using these conventional methods, a great number of accumulation records were developed from ice cores over the past decades, covering decades to centuries (e.g., Alley et al., 1993; Dahl-Jensen et al., 1993; Hardy et al., 2003; Henderson et al., 2006; Hou et al., 2002; Kaspari et al., 2008; Yao et al., 2008). However, it remains challenging to develop annually resolved accumulation records covering longer (e.g. millennial) time periods, because of the difficulties in identifying annual layers and obtaining accurate chronologies in the deeper part of alpine ice cores due to rapid thinning (Roberts et al., 2015; Winstrup et al., 2012). During the past two decades, several effective methods, for example, the continuous flow analysis (CFA) technology and the Laser Ablation Inductively Coupled Plasma Mass Spectrometry (LA-ICP-MS) technology, were developed to measure the chemicals preserved in ice cores with millimeter to sub-millimeter sampling resolution. The resulting ultra-high resolution records could resolve seasonal signals of chemical constituents in ice cores, and were increasingly used to accurately discern annual layers of ice cores from Antarctica, Greenland, and the Alps (Bohleber et al., 2018; Clifford et al., 2019; Haines et al., 2016; Massam et al., 2017; More et al., 2017; Winstrup et al., 2019). The remaining challenge for reconstructing long-term accumulation records thus lies in establishing accurate thinning parameters, and this is largely dependent on the reliable dating of ice cores, particularly at deeper sections. Recently, a novel method was developed to extract water-insoluble organic carbon (WIOC) particles at microgram level from carbonaceous aerosol embedded in the glacier ice for accelerator mass spectrometry (AMS) ^{14}C dating (Uglietti et al., 2016). Carbonaceous aerosols are constantly transported to high-altitude glaciers, where they are deposited and eventually incorporated into the glacier ice. Consequently, carbonaceous aerosols in ice cores can provide reliable dating at any given depth when the samples contain sufficient WIOC (> 10 μg). These dates can then be used to constrain an ice flow model to estimate the mean accumulation rate and thinning parameter of ice cores.

In this study, we propose a new method to establish annual accumulation records of past millennia, taking three sections from an ice core drilled at the Chongce ice cap in the northwestern Tibetan Plateau (TP) as an example (Fig. S1). First, we measured the concentration of aluminum (Al), calcium (Ca), iron (Fe), sodium (Na), magnesium (Mg), copper (Cu), and lead (Pb) from three sections of the Chongce ice core using the LA-ICP-MS technology. It is worth noting that this is the first time to perform the ultra-high-resolution LA-ICP-MS measurement for Tibetan ice cores. Based on the seasonal cycles of these elements, we identified annual layers in the ice core and measured their thickness. Second, we derived

删除了: e.g.,

删除了: reveal

删除了: the

the thinning parameter and the mean accumulation rate of the entire Chongce ice core using a two-parameter steady state flow model constrained by the ^{14}C ages and the ages of other reference layers (e.g., β activity peak). Based on the results, we calculated the modeled annual layer thickness for mean accumulation at different depths. Finally, we derived the actual accumulation for each annual layer within the three sample sections as the product of the ratio of the observed to modeled annual layer thickness and the average annual accumulation of this ice core. It is worth noting that this is also the first time that annual layer identification based on seasonal cycles of LA-ICP-MS intensity of multiple elements is combined with annual layer thinning modeling to reconstruct annual precipitation records at the millennial time scale from the Tibetan ice cores. In addition, we verified the reliability of this method by comparing our results with other reconstructed and modeled precipitation series for the TP.

删除了: W

2 Materials and methods

2.1 The Chongce ice cores

删除了: Retrieval and analysis of t

The Chongce ice cap is located in the western Kunlun Mountains on the northwestern TP (Fig. 1), covering an area of 163.06 km^2 with a volume of 38.16 km^3 (Shi, 2008). The ice cap faces south with a mean equilibrium line altitude of 5900 m above sea level (a.s.l.) (Fig. 1). Climate of the Chongce ice cap and its vicinity is largely controlled by the strength of the mid-tropospheric westerlies (Pang et al., 2020) (Fig. S1). Based on the High Asia Refined analysis (HAR) data (available at: https://www.klima.tu-berlin.de/)(Maussion et al., 2014), precipitation over the Chongce ice cap is highly seasonal (Fig. S2 and S3). Summertime precipitation accounts for ~28% of the annual total, whereas the amount from December to May accounts for ~59% (Fig. S3 and S4). Autumn (September to November) has the lowest amount (13%) of precipitation.

删除了: S

删除了: S

删除了: 2

In October 2012, we retrieved two ice cores to bedrock with lengths of 134.03 m (Core 1, 35°14′5.77″N, 81°7′15.34″E, 6010 m a.s.l.) and 135.81 m (Core 2, 35°14′6.11″N, 81°6′50.62″E, 6010 m a.s.l.) and a shallow ice core with a length of 58.82 m (Core 3, 35°14′5.69″N, 81°6′51.71″E, 6010 m a.s.l.) from the Chongce ice cap with an electromechanical drill. The distance between the drilling sites of Core 2 and Core 3 is ~2 meters. In October 2013, two more ice cores to bedrock were recovered from the Guozha glacier on the same ice cap with lengths of 216.61 m (Core 4, 35°14′56.58″N, 81°5′27.70″E, 6105 m a.s.l.) and 208.63 m (Core 5, 35°14′56.00″N, 81°5′28.06″E, 6104 m a.s.l.) (Fig. S1). Borehole

temperatures are -12.8, -12.6 and -12.6 ℃ at 10 m depth for Core 1, Core 2, and Core 3, and -8.8 and -8.8 ℃ at 130 m depth for Core 1 and Core 2, respectively (Fig. S4), suggesting that the Chongce ice cap is frozen to the bedrock (Hou et al., 2018). The density profiles of Core 2, Core 3, and Core 4 are shown in Fig. S5. All the ice cores were kept frozen and transported to the cold laboratory (-20℃) at Nanjing University for further processing.

2.2 The LA-ICP-MS analysis

The LA-ICP-MS analysis was conducted at the W. M. Keck Laser Ice Core Facility of the Climate Change Institute, the University of Maine, following procedures presented by Sneed et al. (2015) and Spaulding et al. (2017). The system includes the following components: a Thermo Element 2 ICP-MS (Thermo Fisher Scientific, Bremen, Germany) coupled to a standard New Wave UP-213 laser ablation system (New Wave Research, Fremont, California, USA); and the Sayre Cell™, a cryocell chamber designed to hold 1 m of ice at a temperature of -15 ℃. The chamber is equipped with a small (~ 5 cm^3) open-design ablation chamber for continuous ablation of ice core samples at close to their original length (Spaulding et al., 2017).

We selected three trial sections from Core 2 (Section I, II, and III) for the ultra-high resolution LA-ICP-MS analysis, as well as the top section of Core 3 (Top Section) for conventional chemical analysis (~ 3 cm sampling resolution) for comparison (An et al., 2016). The depths of these sections are 0-10.030 m for the Top Section (Core 3), 72.645-73.151 m for Section I, 107.977-108.389 m for Section II, and 122.670-123.032 m for Section III (Core 2) (An et al., 2016). Prior to analysis, Section I, II, and III were split axially into two halves using a band saw. One half was stored as an archive. For the remaining half, we first scraped the surface (longitudinal section) with a Lie Nielson stainless-steel blade to remove possible contamination caused by previous sample preparation. The ice sample was then placed in the W.M. Keck Laser Ice Facility Sayre Cell™ whilst the system was purged with Argon (Ar) gas for two minutes to remove impurities in the system. To save analysis time, the multi-element method of LA-ICP-MS analysis (Spaulding et al. 2017) was used to measure Na, Mg, Cu, and Pb from an ablated line along the surface of the ice core, and Al, Ca, Fe from a parallel line. These two ablated lines were separated by 200 μm to prevent any possible overlap. The sampling resolution is 153 μm per sample. The unit of LA-ICP-MS measurements is intensity (counts per second (cps)).

删除了: 5

删除了: 6

删除了: Ultra-high resolution glaciochemical analysis of the Chongce ice core using

删除了:

删除了: CellTM

删除了:

删除了: the Argon (Ar) gas flow was purged for two minutes to remove impurities in the system

2.3 The β activity measurements

Thirty-one samples were collected successively from the top to a depth of 14.805 m of the Chongce Core 3 (Table S1). Each sample is about 1 kg. The β activity was measured using an Alpha-Beta Multidetector (Mini 20, Eurisys Mesures) at the State Key Laboratory of Cryospheric Science, Lanzhou, China. Details about β activity measurements can be found in An et al. (2016).

2.4 The ^{14}C measurements

The ^{14}C measurements were made at the Paul Scherrer Institut and the University of Bern (LARA laboratory), Switzerland. Nine samples from the Chongce Core 2 were selected for ^{14}C dating (Hou et al., 2018) using a method based on ^{14}C determination in the water-insoluble organic carbon fraction (WIOC) of the aerosols in the ice (Sigl et al., 2009). In Brief, we first decontaminated the ice for the ^{14}C samples by removing the ~3 mm outer layer using a stainless steel bandsaw in a cold room (-20°C) and rinsing the remaining ice core samples with ultrapure water (MilliQ, 18.2 MΩ*cm quality) in a laminar flow hood. The samples were then melted to collect the water-insoluble carbonaceous particles contained in the ice were by filtration. The filters were subsequently combusted at 340°C and then 650°C to separate organic carbon (OC) from element carbon (EC). The resulting CO_2 was measured by the Mini Carbon Dating System (MICADAS) with a gas ion source for ^{14}C analysis. Details about sample preparation and WIOC separation can be found in Uglietti et al. (2016). The overall procedural blanks were estimated using artificial ice blocks of frozen ultra-pure water, which were treated the same way as real ice samples. The average overall procedural blank is 1.34 ± 0.62 μg carbon with a $F^{14}C$ of 0.69 ± 0.13 (Uglietti et al., 2016). The conventional ^{14}C ages were calibrated using OxCal v4.4 online program (https://c14.arch.ox.ac.uk/) (Ramsey and Lee, 2013) with the IntCal13 calibration curve (Reimer et al., 2013). Results of the individual samples can be found in Table S2.

2.5 Annual-layer identification using the StratiCounter program

In comparison to our visual annual-layer results, we applied the StratiCounter program to identify annual layers for Section III. The StratiCounter program is an automated annual-layer detection method based on the Hidden Markov Model (HMM) algorithms (Winstrup et al., 2012). The code for the StratiCounter program is available at the github repository (http://www.github.com/maiwinstrup/StratiCounter).

删除了: Twenty-two

删除了: W

删除了: box

删除了: the previous studies (

删除了: ,

删除了: Bronk

删除了: To verify

删除了: identification

删除了: is

2.6 The TraCE-21ka simulation

For comparison, we also used data from the "Simulation of Transient Climate Evolution over the Last 21,000 years" (TraCE-21ka) (Collins et al., 2006; Liu et al., 2009). The TraCE-21ka experiment was performed using a coupled ocean-atmosphere model, the Community Climate Model version3 (CCSM3), forced by realistic variations in insolation, atmospheric greenhouse gases (GHGs), meltwater fluxes and continental ice sheets. The atmospheric resolution is 3.75° × 3.75° horizontally, with 26 vertical levels. we calculated annual precipitation in the western Kunlun Mountains covering the last three millennia based on outputs from the TraCE-21ka climate simulation (available at: https://www.earthsystemgrid.org).

删除了： state-of-the-art

3 Results

3.1 Annual-layer identification using multiple chemical species

Various chemical species obtained from Tibetan ice cores exhibit distinct seasonal cycles (An et al., 2016; Thompson et al., 2018). On the northwestern TP, the $\delta^{18}O$ values in modern precipitation show distinct seasonal fluctuations with high values in summer and low values in winter (Thompson et al., 2018). In addition, chemical elements (e.g., Al, Ca, Fe, and Mg) also show marked seasonal cycles with high concentrations in late winter and spring and low concentrations in summer (Thompson et al., 2018).

In this paper, annual layers of the Top Section were identified based on seasonal cycles of $\delta^{18}O$ values (Fig. 1). The distance between two adjacent low $\delta^{18}O$ values was defined as the annual layer thickness (An et al., 2016). The result was verified by a reference of β activity peak in 1963 A.D. due to thermonuclear bomb testing, and a second β activity peak in 1986 A.D. corresponding to the Chernobyl nuclear accident. The derived average annual layer thickness of the Top Section is 168.61 ± 61.91 mm (corresponding to 140.76 ± 48.56 mm w.e.) (Fig. 1). Annual layers of Section I, II, and III were identified based on seasonal cycles of Al, Ca, Fe, Mg. In these sections, annual layer boundaries were defined as synchronous local maxima in all the four element concentrations. In addition, we follow the approach successfully employed for Greenland ice cores by Rasmussen et al. (2006) to quantify counting uncertainty from uncertain layers. In this approach, we count uncertain layers as 0.5 ± 0.5 years, and estimate the maximum counting error (MCE) from the number of uncertain layers (N) as N × 0.5 years. Using the records for four elements (i.e., Al, Ca, Fe, Mg), we define "uncertain annual layer boundaries"

as those without synchronous peaks of all four elements. Annual layer peaks for each of the three sections and their respective uncertainties are shown in Fig. 2. The number of annual layers for Section I, II, and III is 8 ± 2, 19 ± 3, and 23 ± 3. The derived average annual layer thickness for Section I, II, and III is thus $38.30 \pm {}^{9.57}_{6.38}$ mm (corresponding to $30.96 \pm {}^{7.74}_{5.16}$ mm w.e.), $18.42 \pm {}^{3.45}_{2.51}$ mm ($14.74 \pm {}^{2.76}_{2.01}$ mm w.e.), and $12.71 \pm {}^{1.91}_{1.47}$ mm ($10.16 \pm {}^{1.52}_{1.17}$ mm w.e.), respectively.

We also applied the StratiCounter program to identify annual layers objectively for Section III (Fig. S6). Despite minor differences, StratiCounter produced mostly comparable results. The average annual layer thickness derived from the StratiCounter counts is 12.60 mm (corresponding to 10.08 mm w.e.), which is roughly consistent with our estimate from the manual layer counting ($10.16 \pm {}^{1.52}_{1.17}$ mm w.e.). This confirms the reliability of our manual layer counting. The StratiCounter program could not be applied to Sections I and II due to their short duration. For consistency, we used results from manual layer counting for further analysis and discussion.

3.2 Thinning of annual layers due to ice flow

Glaciers consist of sequences of sedimentary deposits of annual snow in polar and alpine regions (Rapp, 2012). Snow layers sink into the ice mass and are subjected to continuous thinning (Nye, 1963; Rapp, 2012). This occurs initially due to densification, by which the snow is gradually transformed into ice, but later mainly because of flow induced vertical compressive strain. Therefore, the observed thickness of an annual layer reflects both the initial amount of annual accumulation and the vertical compression the layer has been subject to since deposition (Paterson and Waddington, 1984). In this process, the ice layers are stretched horizontally until they are advected by the ice motion into an ablation zone (Rapp, 2012). The Chongce Core 2 was drilled on a flat platform with an area of over 160 km^2 where the ice layers are horizontal. As a result, horizontal deformation has little effect on the redistribution of snow. In addition, temporal changes in basal topography are likely minimal due to Holocene origin of the Chongce Core 2 (Hou et al., 2018; Licciulli et al., 2020). Therefore, here we estimated the vertical strain rate and accumulation rate of the Chongce Core 2 using a simple two-parameter steady state flow model (Bolzan, 1985):

$$T_{(z)} = \frac{H}{bp}\left[\left(1 - \frac{z}{H}\right)^{-p} - 1\right].$$

The model has two degrees of freedom, the net annual accumulation rate b and the thinning parameter p, both of which are assumed to be constant over time. H is the glacier thickness (m w.e.). z is the depth (m

删除了： In these sections, the LA-ICP-MS profile of each element (Al, Ca, Fe, and Mg) is characterized by the regular occurrence of several distinct peaks grouped together, along with an elevated baseline of each element's concentration (Fig. S7). The groups of peaks are separated by a prolonged section of low element concentrations (Fig. 1 and S7). The grouped peaks are interpreted as independent snow events of elevated element concentrations during the winter/spring (Fig. S7). The periods of low values correspond to snow deposition during the summer (Fig. S7). Annual layer boundaries of Section I, II, and III were defined as the local maxima (maximum in each group of peaks) in the concentration of the four elements (Fig. S7). It is worth nothing that seasonal cycles of these elements are not always synchronous, so the identification of annual layers requires expert judgment. Fig. 1 shows annual layer delineation for each of the three sections. The derived average annual layer thickness for Section I, II, and III is 47.73 ± 16.98 mm (corresponding to 38.59 ± 13.73 mm w.e.), 19.24 ± 3.66 mm (corresponding to 15.39 ± 2.93 mm w.e.), and 11.92 ± 3.92 mm (corresponding to 9.53±3.13 mm w.e.) respectively.

删除了： To verify our layer identification, w

删除了： 8

删除了： This is an automated annual-layer detection method based on the Hidden Markov Model (HMM) algorithms (Winstrup et al., 2012). …

删除了： large

删除了： 11.15 ± 4.84

删除了： 8.92 ± 3.87

删除了： about 6.5% lower than

删除了：

删除了： s

删除了： ; Nye, 1963

w.e.), and $T_{(z)}$ is the corresponding age at *z*. For the Chongce Core 2 (drilled to bedrock), *H* is 112.243 m water equivalent (m w.e.), calculated as the product of the ice core length and its density. In order not to overweigh the data by the deepest horizons, the model is fitted using the logarithms of the age values (Uglietti et al., 2016). The model was first constrained by the ^{14}C calibrated ages, together with the *β*-activity reference horizon of the Chongce 58.82 m Core 3, located only ~ 2 meters apart (Hou et al., 2018; Pang et al., 2020). We found that by using these data only, the model is poorly constrained at the deep section, and giving an estimate bottom age much older than the bottom age (8.3 ± $^{6.2}_{3.6}$ ka B.P.) estimated for Core 4 (Hou et al., 2018). Therefore, we included the Core 4 bottom age to constrain the final model. Due to its mathematical configuration to account for ice flow dynamics, the model gives more weight to points at shallower sections. Therefore, the inclusion of the Core 4 bottom age (relatively younger than otherwise derived bottom age) pushes the curve towards the left (younger) of most ^{14}C dates (Fig. 3). The derived thinning parameter is 0.008 (dimensionless), and average annual accumulation of the entire ice core (~ 9 ka to present) is 103 ± 34 mm w.e. (Fig. 3). This derived accumulation rate is in relative agreement with the average annual accumulation which was observed in the uppermost 50 annual layers (~ 140 mm w.e./year) where the thinning effect is negligible (Hou et al., 2018). The derived ice age at the bedrock is 9.0 ± $^{7.9}_{3.6}$ ka B.P., which is roughly consistent with the bottom age (8.3 ± $^{6.2}_{3.6}$ ka B.P.) estimated for Core 4. In addition, the modeled age at the depth of the oldest ^{14}C sample is 5.2 ± $^{1.9}_{1.4}$ ka B.P., similar to the actual ^{14}C age of 6.3 ± 0.2 ka B.P. given the uncertainty range. Therefore, we believe this model gives the most reasonable results, compared with several other model fit based on different data combinations (Fig. S7). Details of these model fits are provided in Text S1 and Fig. S7.

3.3 Accumulation rates of the past four time windows

With the derived thinning parameter and average annual accumulation over the Holocene, we calculated the initial annual layer thickness (mm w.e.) for the average accumulation rate at various depths for the Top Section, Section I, II, and III using a simple flow model for the decrease of the annual layer thickness with depth (Bolzan, 1985; Uglietti et al., 2016):

$$L_{(z)} = b(1 - \frac{z}{H})^{1+p},$$

where $L_{(Z)}$ is the modeled annual layer thickness (mm w.e.) for the average accumulation rate (*b*, i.e., 103±34 mm w.e.) at the depth of *z* given the thinning parameter of *p* (i.e., 0.008). The modeled annual

删除了： not

删除了: from

删除了: Using the established ^{14}C ages and the ages of other reference layers, we can fit the model by a nonlinear least squares approach. The set of known *z* and $T_{(z)}$ are summarized in Table S1. The derived thinning parameter is 0.008 (dimensionless), and average annual accumulation of the entire ice core (~ 9 ka to present) is 103 ± 34 mm w.e. (Fig. 2). This accumulation rate is in relative agreement with the average annual accumulation which was observed in the uppermost 50 annual layers (~ 140 mm w.e./year) where the thinning effect is negligible (Hou et al., 2018). In addition, the modeled age at the depth of the oldest ^{14}C sample is 5.2±$^{1.9}_{1.4}$ ka B.P., similar to the actual ^{14}C age of 6.3 ± 0.2 ka B.P. given the uncertainty range. Therefore, the assumption of constant accumulation (*b*) and a constant thinning parameter (*p*) over time/with depth is reasonable.

删除了: of

删除了:)

删除了: .

layer thickness ranges 95.27-102.94 mm w.e. for the Top Section (corresponding to 1951-2012 A.D.), 47.01-47.30 mm w.e. for Section I (corresponding to 781-789 a B.P.), 20.73-20.76 mm w.e. for section II (corresponding to 1682-1697 a B.P.), and 9.49-9.73 mm w.e. for section III (corresponding to 2511-2541 a B.P.). The estimated original (pre-thinning) accumulation (mm w.e.) for each annual layer can be derived through multiplying the ratio of the observed to modeled annual layer thickness (mm w.e.) by the average annual accumulation rate (103 mm w.e.) (Hou et al., 2018; Roberts et al., 2015; Winstrup et al., 2012). The observed layer thickness is established in section 3.1. The results (Fig. 4) show that the mean annual accumulation was $108.86 \pm ^{16.29}_{12.54}$ mm w.e. at ~ 2.5 ka B.P., which is comparable to the Holocene mean value. The mean annual accumulation was $73.73 \pm ^{13.80}_{10.05}$ mm w.e. at ~1.7 ka B.P. and $67.62 \pm ^{16.91}_{11.27}$ mm w.e. at ~ 0.8 ka B.P., about 28% and 34% lower than the Holocene mean respectively. The mean annual accumulation was 146.30 mm w.e. during 1953-2012 A.D., ~ 42% higher than the Holocene mean.

4 Discussion

Alpine glaciers over the TP extend high into the middle troposphere, yielding ice cores that provide continuous annual accumulation records representative of a large area (Duan et al., 2015; Yao et al., 2008). However, not all snowfall is securely stored in high-elevation glaciers, due to wind scouring, snow drifting, and sublimation (Hardy et al., 2003). Moreover, firnification process might develop rapidly as indicated from the lack the lower density layers (indicative of snow) near the glacier surface (Fig. S5). Therefore, ice core accumulation reconstructed in this paper is not a direct measurement of precipitation but rather a quantitative proxy of net precipitation in the western Kunlun Mountains. In Fig. 4, the reconstructed average annual accumulation of the four time windows was compared with other reconstructed and modeled precipitation series for the TP to evaluate the reliability of our method of reconstruction. Thompson et al. (1995) reconstructed a snow accumulation record for the last millennium from an ice core retrieved at the Guliya ice cap (~ 30 km from the Chongce drilling site). Their reconstruction shows that snow accumulation rate for 1950-1989 A.D. (32.18 cm ice/year) is 62% higher than that for 1160-1169 A.D. (19.79 cm ice/year) (Fig. 4b). This is largely consistent with the Chongce reconstruction, which shows a 65% increase in the mean annual accumulation between 1160-1172 A.D (84.28 mm w.e.) and 1953-1989 A.D (139.03 mm w.e.). Yang et al. (2014) reconstructed annual

删除了: initial

删除了: 3

删除了: It

删除了: 76.45 ± 14.52

删除了: 84.26 ± 29.85

删除了: 5

删除了: 18

删除了: A

删除了: 146.38 ± 50.45

删除了: can be

删除了:

删除了: 3

删除了: 2006

删除了: 3

precipitation over the past 3500 years using subfossil, archaeological, and living juniper tree samples from the northeastern TP (Fig. 4c). Their reconstruction shows that the last 50 years is a very wet period relative to the past 3500 years, consistent with our reconstruction. In addition, both records show similar dry intervals in ~ 0.8 ka B.P. and ~ 1.7 ka B.P. and a moderately wet interval at ~ 2.5 ka B.P. (Fig. 4). Our reconstruction is also in agreement with the TraCE-21 ka model results (extracted for the study region of 34-36°N, 80-82°E), which simulate continuous climate evolution over the last 21,000 years (Collins et al., 2006) (Fig. 4d). These results suggest that the method proposed in this study produces reliable results and has the potential to reconstruct high-resolution continuous precipitation time series.

Compared with the previous precipitation records based on paleoclimate proxies such as tree-ring width, pollen abundance index, ice core chemistry, and stalagmites, the method proposed in this paper has the significant advantage in quantifying annually-resolved precipitation of past millennia. Previous quantitative precipitation reconstructions assume a stationary linear relationship between proxy data and actual precipitation over time (Tozer et al., 2016; Yang et al., 2014), which is difficult to establish over long periods. In comparison, net accumulation rates in ice cores provides more direct and quantitative data for past precipitation. The establishment of a reliable annual accumulation record is determined only by two factors: (i) identification of the annual layers and (ii) the ice core thinning parameters. Moreover, ice core accumulation records could be used to quantify annual precipitation over Antarctica and the Greenland ice cap, where no other precipitation proxies exist.

The reliability of this method can be further improved with the existence of absolute chronological markers (e.g., volcanic events and archaeological archives). If such markers exist in an ice core, a local average annual layer thickness (b) can be calculated between two adjacent markers by dividing the length of ice by the number of annual layers between them. The average net annual accumulation can then be determined from ratio of the average net annual layer thickness (mm w.e.) to the flow-modeled thickness (mm w.e.) multiplied by the average annual accumulation of the Holocene. This provides an additional way to verify the reconstructed accumulation rates. As a result, we can improve the reliability of our method by comparing three different reconstructions (i.e., the Holocene net mean accumulation derived from the two-parameter model, average net annual accumulation between adjacent absolute chronological markers, and average net annual accumulation of different time windows based on annual layer identification). In addition, we will perform more direct observations (e.g., surface and bedrock topography and borehole inclination angles) on the Chongce ice cap in the future and use them to

删除了: 3

删除了: 3

删除了: 3

删除了: Therefore, comparison of the average annual accumulation of each section with the Holocene average was not influenced by the error of ice core chronology caused by two-parameter flow model.

constrain a state-of-the-art 3-D ice core model (Licciulli et al., 2020). This could further improve our estimates of accumulation rate and the thinning parameter.

5 Conclusions

In this paper, we presented a new method to quantify annual accumulation from alpine ice cores for past millennia, using as an example an ice core drilled at the Chongce ice cap in the northwestern TP. We used the LA-ICP-MS technology to develop continuous ultra-high-resolution records of chemical constituents (Al, Ca, Fe, Na, Mg, Cu, and Pb) in three sections of the Chongce ice core (corresponding to 781-789 a B.P., 1682-1697 a B.P., and 2511-2541 a B.P in age respectively). Based on the seasonality shown in these trace element records (Al, Ca, Fe, and Mg), we identified annual layers in each section. In addition, annual layers of the Top Section of Chongce ice core (1953-2012 A.D. in age) were identified based on seasonal cycles of $\delta^{18}O$ values. The thickness of these annual layers was subsequently corrected using a two-parameter flow model to establish initial net accumulation for these sections. The results show that the average annual accumulation was 109 mm around 2.5 ka B.P., which is comparable to the Holocene average. The average accumulation was 74 mm at 1.7 ka B.P. and 68 mm at 0.8 ka B.P., about 28% and 34% lower than the Holocene average. It reached a high value of 145 mm during 1953-2012 A.D., about 41% higher than the Holocene average. Our estimates are consistent with previous results from tree rings and the TraCE-21 ka transient model simulations. Therefore, the method has the potential to reconstruct continuous high resolution precipitation records covering millennia or even longer time periods.

删除了: 2

删除了: 6

删除了: 84

删除了: 26

删除了: 18

Data availability. The data used in this paper can be downloaded from the Zenodo website (http://doi.org/10.5281/zenodo.4387022).

Author contributions. SH conceived this study and drilled the ice cores. WZ and EVK took the measurements. WZ wrote the paper. All authors contributed to discussion of the results.

Competing interests. The authors declare no conflict of interest.

Acknowledgments

Many thanks are due to many scientists, technicians, graduate students and porters, especially to Yongliang Zhang, Hao Xu, and Yaping Liu, for their great efforts working at high elevations, to Mariusz Potocki for his help in measuring chemical constituents of ice core samples, to Chiara Uglietti and Heinz Walter Gäggeler for help in measuring the ^{14}C samples, and to Guocai Zhu for providing the ground-penetrating radar results. In China, this work was supported by the National Natural Science Foundation of China (91837102, 41830644, 42021001, and 42001050). In USA, the Climate Change Institute's W.M. Keck Laser Ice Facility and their ICP-MS laboratory at the University of Maine gratefully acknowledges support for this facility from the W. M. Keck Foundation and US National Science Foundation (PLR-042883, PLR-1203640, and PLR-1417476).

删除了:

删除了: The data for the work in this paper can be downloaded from the Zenodo website (available from: http://doi.org/10.5281/zenodo.4387022).

References

An, W., Hou, S., Zhang, W., Wu, S., Xu, H., Pang, H., Wang, Y., and Liu, Y.:. Possible recent warming hiatus on the northwestern Tibetan Plateau derived from ice core records, Sci. Rep., 6, 32813, https://doi.org/10.1038/srep32813, 2016.

Alley, R. B., Meese, D. A., Shuman, C. A., Gow, A. J., Taylor, K. C., Grootes, P. M., White, J. W. C., Ram, M., Waddington, E. D., Mayewski, P. A., and Zielinski, G. A.: Abrupt increase in Greenland snow accumulation at the end of the Younger Dryas event, Nature, 362, 527–529, https://doi.org/10.1038/362527a0, 1993.

Bohleber, P., Erhardt, T., Spaulding, N., Hoffmann, H., Fischer, H., and Mayewski, P.: Temperature and mineral dust variability recorded in two low-accumulation Alpine ice cores over the last millennium, Clim. Past, 14, 21–37, https://doi.org/10.5194/cp-14-21-2018, 2018.

Bolzan, J. F.: Ice flow at the Dome C ice divide based on a deep temperature profile, J. Geophys. Res., 90(D5), 8111–8124, https://doi.org/10.1029/JD090iD05p08111, 1985.

Cai, Y., Zhang, H., Cheng, H., An, Z., Edwards, R. L., Wang, X., Tan, L., Liang, F., Wang, J., and Kelly, M.: The Holocene Indian monsoon variability over the southern Tibetan Plateau and its teleconnections, Earth Planet. Sci. Lett., 335–336, 135–144, https://doi.org/10.1016/j.epsl.2012.04.035, 2012.

Clifford, H. M., Spaulding, N. E., Kurbatov, A. V., More, A., Korotkikh, E. V., Sneed, S. B., Handley, M., Maasch, K. A., Loveluck, C. P., Chaplin, J., McCormick, M., and Mayewski, P. A.: A 2000 year Saharan dust event proxy record from an ice core in the European Alps, J. Geophys. Res. Atmos., 124, 12882–12900, https://doi.org/10.1029/2019JD030725, 2019.

Collins, W. D., Bitz, C. M., Blackmon, M. L., Bonan, G. B., Bretherton, C. S., Carton, J. A., Chang, P., Doney, S. C., Hack, J. J., Henderson, T. B., Kiehl, J. T., Large, W. G., McKenna, D. S., Santer, B. D., and Smith, R. D.: The Community Climate System Model Version 3 (CCSM3), J. Climate, 19(11), 2122–2143, https://doi.org/10.1175/JCLI3761.1, 2006.

Dahl-Jensen, D., Johnsen, S. J., Hammer, C. U., Clausen, H. B., and Jouzel, J.: Past Accumulation rates derived from observed annual layers in the GRIP ice core from Summit, Central Greenland, in: Ice in the Climate System, edited by: Peltier, W. R., NATO ASI Series, 12, 517–532, https://doi.org/10.1007/978-3- 642-85016-5_29, 1993.

Duan, K., Xu, B., and Wu, G.: Snow accumulation variability at altitude of 7010 m a.s.l. in Muztag Ata Mountain in Pamir Plateau during 1958–2002. J. Hydrol., 531, 912–918, https://doi.org/10.1016/j.jhydrol.2015.10.013, 2015.

Haines, S. A., Mayewski, P. A., Kurbatov, A. V., Maasch, K. A., Sneed, S. B., and Spaulding, N.: Ultra-high resolution snapshots of three multi-decadal periods in Antarctic ice core, J. Glaciol., 62(231), 31–36, https://doi.org/10.1017/jog.2016.5, 2016.

Hardy, D. R., Vuille, M., and Bradley, R. S.: Variability of snow accumulation and isotopic composition on Nevado Sajama, Bolivia. J. Geophys. Res, 108(D22), https://doi.org/10.1029/2003JD003623, 2003.

删除了： Bronk Ramsey, C., and Lee, S.: Recent and planned developments of the program Oxcal, Radiocarbon, 55, 720–730. https://doi.org/10.1017/S0033822200057878, 2013.

删除了： Christiansen, B., and Ljungqvist, F. C.: Challenges and perspectives for large-scale temperature for large-scale temperature reconstructions of the past two millennia, Rev. Geophys., 55, 40–96, https://doi.org/10.1002/2016RG000521, 2017.

Henderson, K., Laube, A., Gäggeler, H. W., Olivier, S., Papina, T., and Schwikowski, M.: Temporal variations of accumulation and temperature during the past two centuries from Belukha ice core, Siberian Altai, J. Geophys. Res., 111, D03104, https://doi.org/10.1029/2005JD005819, 2006.

Hou, S., Qin, D., Yao, T., Zhang, D., and Chen, T.: Recent change of the ice core accumulation rates on the Qinghai-Tibetan Plateau, Chinese Sci. Bull., 47(20), 1746–1749, https://doi.org/10.1360/02tb9382, 2002.

Hou, S., Jenk, T. M., Zhang, W., Wang, C., Wu, S., Wang, Y., Pang, H., and Schwikowski, M.: Age ranges of the Tibetan ice cores with emphasis on the Chongce ice cores, western Kunlun Mountains, The Cryosphere, 12, 2341–2348, http://doi.org/10.5194/tc-12-2341-2018, 2018.

Kaspari, S., Hooke, R. L., Mayewski, P. A., Kang, S., Hou, S., and Qin, D.: Snow accumulation rate on Qomolangma (Mount Everest), Himalaya: synchroneity with sites across the Tibetan Plateau on 50–100 year timescale, J. Glaciol., 54(185), 343–352, https://doi.org/10.3189/002214308784886126, 2008.

Kidd, C., and Huffman, G.: Global precipitation measurement, Meteorol. Appl., 18, 334–353, https://doi.org/10.1002/met.284, 2011.

Liu, Z., Otto-Bliesner, B. L., He, F., Brady, E. C., Tomas, R., Clark, P. U., Carlson, A. E., Lynch-Stieglitz, J., Curry, W., Brook, E., Erickson, D., Jacob, R., Kutzbach, J., and Cheng, J.: Transient Simulation of Last Deglaciation with a New Mechanism for Bølling-Allerød Warming, Science, 325(5938), 310–314, https://doi.org/10.1126/science.1171041, 2009.

Licciulli, C., Bohleber, P., Lier, J., Gagliardini, O., Hoelzle, M., and Eisen, O.: A full Stokes ice-flow model to assist the interpretation of millennial-scale ice cores at the high-Alpine drilling site Colle Gnifetti, Swiss/Italian Alps, J. Glaciol., 66(255), 35–48, https://doi.org/10.1017/jog.2019.82, 2020.

Massam, A., Sneed, S. B., Lee, G. P., Tuckwell, R. R., Mulvaney, R., Mayewski, P. A., and Whitehouse, P. L.: A comparison of annual layer thickness model estimates with observational measurements using the Berkner Island ice core, Antarctica, Antarct. Sci., 29(4), 382–393, https://doi.org/10.1017/S0954102017000025, 2017.

Maussion, F., Scherer, D., Mölg, T., Collier, E., Curio, J., and Finkelnburg, R.: Precipitation seasonality and variability over the Tibetan Plateau as resolved by the High Asia Reanalysis, J. Climate, 27(5), 1910–1927, https://doi.org/10.1175/JCLI-D-13-00282.1, 2014.

More, A. F., Spaulding, N. E., Bohleber, P., Handley, M. J., Hoffmann, H., Korotkikh, E. V., Kurbatov, A. V., Loveluck, C. P., Sneed, S. B., McCormick, M., and Mayewski, P. A.: Next generation ice core technology reveals true minimum natural levels of lead (Pb) in the atmosphere: Insights from the black death, GeoHealth, 1, 211– 219, https://doi.org/10.1002/2017GH000064, 2017.

Nye, J. F.: Correction Factor for Accumulation Measured by the Thickness of the Annual Layers in an Ice Sheet, J. Glaciol., 4, 785–788, https://doi.org/10.3189/S0022143000028367, 1963.

Pang, H., Hou, S., Zhang, W., Wu, S., Jenk, T. M., Schwikowski, M., and Jouzel, J.: Temperature Trends in the Northwestern Tibetan Plateau Constrained by Ice Core Water Isotopes Over the Past 7,000 Years, J. Geophys. Res. Atmos., 125(19), e2020JD032560, 2020.

Paterson, W. S. B., and Waddington, E. D.: Past precipitation rates derived from ice core measurements: Methods and data analysis, Rev. Geophys., 22(2), 123–130, https://doi.org/10.1029/RG022i002p00123, 1984.

Ramsey, C. B., and Lee, S.: Recent and planned developments of the program Oxcal, Radiocarbon, 55, 720–730, https://doi.org/10.1017/S0033822200057878, 2013.

Rapp, D.: Glacials and Interglacials: Measurement, Interpretation and Models, Springer-Verlag, Berlin, https://doi.org/10.1007/9783-642-30029-5-11, 2012.

Reimer, P. J., Bard, E., Bayliss, A., Beck, J. W., Blackwell, P. G., Ramsey, C. B., Buck, C. E., Cheng, H., Lawrence Edwards, R., Friedrich, M., Grootes, P. M., Guilderson, T. P., Haflidason, H., Irka Hajdas, I., Hatté, C., Heaton, T. J., Hoffmann, D. L., Hogg, A. G., Hughen, K. A., Kaiser, K. F., Kromer, B., Manning, S. W., Niu, M., Reimer, R. W., Richards, D. A., Scott, E. M., Southon, J. R., Staff, R. A., Turney, C. S. M., and van der Plicht, J.: IntCal13 and marine13 radiocarbon age calibration curve 0–50,000 years cal BP, Radiocarbon, 55, 1869–1887, https://doi.org/10.2458/azu_js_rc.55.16947, 2013.

Roberts, J., Plummer, C., Vance, T., van Ommen, T., Moy, A., Poynter, S., Treverrow, A., Curran, M., and George, S.: A 2000-year annual record of snow accumulation rates for Law Dome, East Antarctica, Clim. Past, 11, 697–707, https://doi.org/10.5194/cp-11-697-2015, 2015.

Shi, Y. (Ed.): Concise Glacier Inventory of China, Shanghai Popular Science Press, China, 2008.

Sigl, M., Jenk, T. M., Kellerhals, T., Szidat, S., Gäggeler, H. W., Wacker, L., Synal, H.-A., Boutron, C., Barbante, C., Gabrieli, J., and Schwikowski, M.: Instruments and methods towards radiocarbon

删除了: Parrenin, F., Rémy, F., Ritz, C., Siegert, M. J., and Jouzel, J.: New modeling of the Vostok ice flow line and implication for the glaciological chronology of the Vostok ice core, J. Geophys. Res., 109, D20202, https://doi.org/10.1029/2004JD004561, 2004.

dating of ice cores, J. Glaciol., 55(194), 985–996, https://doi.org/10.3189/002214309790794922, 2009.

Sneed, S. B., Mayewski, P. A., Sayre, W. G., Handley, M. J., Kurbatov, A. V., Taylor, K. C., Bohleber, P., Wagenbach, D., Erhardt, T., and Spaulding, N. E.: New LA-ICP-MS cryocell and calibration technique for sub-millimeter analysis of ice cores, J. Glaciol., 61(226), 233– 242, https://doi.org/10.3189/2015JoG14J139, 2015.

Spaulding, N. E., Sneed, S. B., Handley, M. J., Bohleber, P., Kurbatov, A. V., Pearce, N. J., Erhardt, T., and Mayewski, P. A.: A new multielement method for LA-ICP-MS data acquisition from glacier ice cores, Environ. Sci. Technol., 51(22), 13282–13287, https://doi.org/10.1021/acs.est.7b03950, 2017.

Sun, Q., Miao, C., Duan, Q., Ashouri, H., Sorooshian, S., and Hsu, K.-L.: A review of global precipitation data sets: Data sources, estimation, and intercomparisons, Rev. Geophys., 56, 79–107, https://doi.org/10.1002/2017RG000574, 2018.

Thompson, L. G., Mosley-Thompson, E., Davis, M. E., Lin, P. N., Dai, J., and Bolzan, J. F.: A 1000 year climate ice-core record from the Guliya ice cap, China: its relationship to global climate variability, Ann. Glaciol., 21, 175–181, https://doi.org/ 10.1017/S0260305500015780, 1995.

Thompson, L. G., Yao, T., Davis, M. E., Mosley-Thompson, E., Wu, G., Porter, S. E., Xu, B., Lin, P. N., Wang, N., Beaudon, E., Duan, K., Sierra-Hernández, M. R., and Kenny, D. V.: Ice core records of climate variability on the Third Pole with emphasis on the Guliya ice cap, western Kunlun Mountains, Quaternary Sci. Rev., 188, 1–14, https://doi.org/10.1016/j.quascirev.2018.03.003, 2018.

Tozer, C. R., Vance, T. R., Roberts, J. L., Kiem, A. S., Curran, M. A. J., and Moy, A. D.: An ice core derived 1013-year catchment-scale annual rainfall reconstruction in subtropical eastern Australia, Hydrol. Earth Syst. Sci., 20, 1703–1717, https://doi.org/10.5194/hess-20-1703-2016, 2016.

Uglietti, C., Zapf, A., Jenk, T. M., Sigl, M., Szidat, S., Salazar, G., and Schwikowski, M.: Radiocarbon dating of glacier ice: overview, optimization, validation, and potential, The Cryosphere, 10, 3091–3105, https://doi.org/10.5194/tc-10-3091-2016, 2016.

Winstrup, W., Svensson, A. M., Rasmussen, S. O., Winther, O., Steig, E. J., and Axelrod, A. E.: An automated approach for annual layer counting in ice cores, Clim. Past, 8, 1881–1895, https://doi.org/10.5194/cp-8-1881-2012, 2012.

删除了： Tang, Y., Pang, H., Zhang, W., Li, Y., Wu, S., and Hou, S.: Effects of changes in moisture source and the upstream rainout on stable isotopes in precipitation—A case study in Nanjing, eastern China, Hydrol. Earth Syst. Sci., 19(10), 4293–4306. https://doi.org/10.5194/hess-19-4293-2015, 2015.
Thompson, L., Mosley-Thompson, E., Brecher, H., Davis, M., León, B., Les, D., Lin, P.-N., Mashiotta, T., and Mountain, K.:Abrupt tropical climate change: Past and present, P. Natl. Acad. Sci. USA, 103(28), 10536-10543, https://doi.org/10.1073/pnas.0603900103, 2006.

Winstrup, M., Vallelonga, P., Kjaer, H. A., Fudge, T. J., Lee, J. E., Riis, M. H., Edwards, R., Bertler, N. A. N., Blunier, T., Brook, E. J., Buizert, C., Ciobanu, G., Conway, H., Dahl-Jensen, D., Ellis, A., Emanuelsson, B. D., Hindmarsh, R. C. A., Keller, E. D., Kurbatov, A. V., Mayewski, P. A., Neff, P. D., Pyne, R. L., Simonsen, M. F., Svensson, A., Tuohy, A., Waddington, E. D., and Wheatley, S.: A 2700-year annual timescale and accumulation history for an ice core from Roosevelt Island, West Antarctica, Clim. Past, 15(2), 751– 779, https://doi.org/10.5194/cp-15-751-2019, 2019.

Xu, T., Zhu, Lü, X., Ma, Q., Wang, J., Ju, J., and Huang, L.: Mid- to late-Holocene paleoenvironmental changes and glacier fluctuations reconstructed from the sediments of proglacial lake Buruo Co, northern Tibetan Plateau, Palaeogeogr. Palaeocl., 517, 74–85, https://doi.org/10.1016/j.palaeo.2018.12.023, 2019.

Yang, B., Qin, C., Wang, J., He, M., Melvin, T. M., Osborn, T. J., and Briffa, K. R. (2014), A 3500-year tree-ring record of annual precipitation on the northeastern Tibetan Plateau, P. Natl. Acad. Sci. USA, 111(8), 2903–2908, https://doi.org/10.1073/pnas.1319238111, 2014.

Yao, T., Duan, K., Xu, B., Wang, N., Guo, X., and Yang, X.: Precipitation record since AD 1600 from ice cores on the central Tibetan Plateau, Clim. Past, 4, 175–180, https://doi.org/10.5194/cp-4-175-2008, 2008.

Zhang, Y., Kang, S., Zhang, Q., Grigholm, B., Kaspari, S., You, Q., Qin, D., Mayewski, P. A., Cong, Z., Huang, J., Sillanpää, M., Chen, F.: A 500 year atmospheric dust deposition retrieved from a Mt. Geladaindong ice core in the central Tibetan Plateau, Atmos. Res., 166, 1–9, https://doi.org/10.1016/j.atmosres.2015.06.007, 2015.

Zhang, Z., Hou, S., and Yi, S.: The first luminescence dating of Tibetan glacier basal sediment, The Cryosphere, 12, 163–168, https://doi.org/10.5194/tc-12-163-2018, 2018.

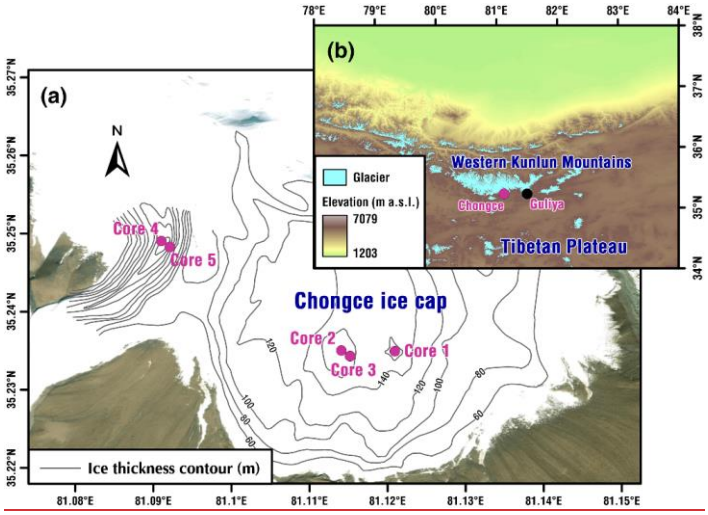

640 **Figure 1.** (a) Satellite image of the Chongce ice cap with location of the ice-core drilling sites (deep rose dots). Ice thickness contours were superimposed on the image of the glacier. (b) Topographic map of the northwestern TP. The satellite imagery map is available at: https://www.mapsofworld.com/satellite-map/world.html. The topographic data were extracted using the Shuttle Radar Topography Mission (SRTM) 90 m DEM digital elevation database, available at: http://srtm.csi.cgiar.org/. Data of glaciers 645 are from the Global Land Ice Measurements from Space (GLIMS; available at: http://www.glims.org).

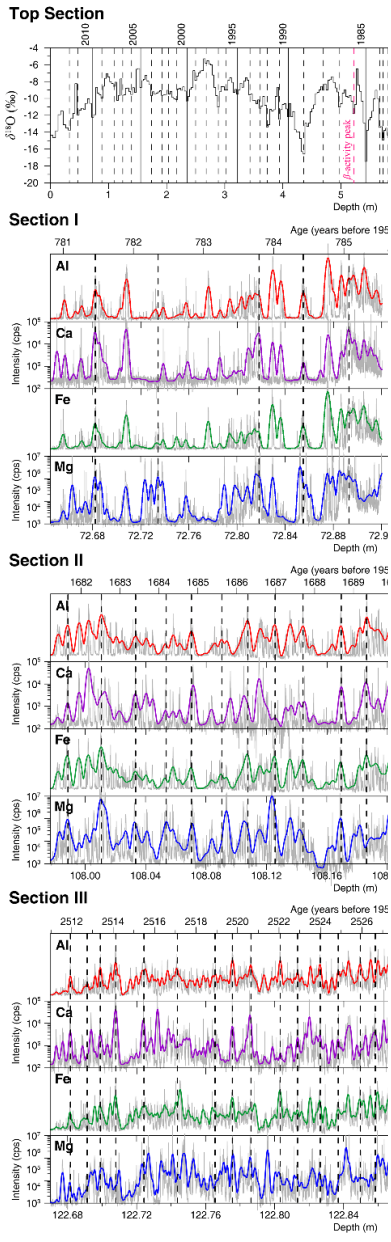

删除了：

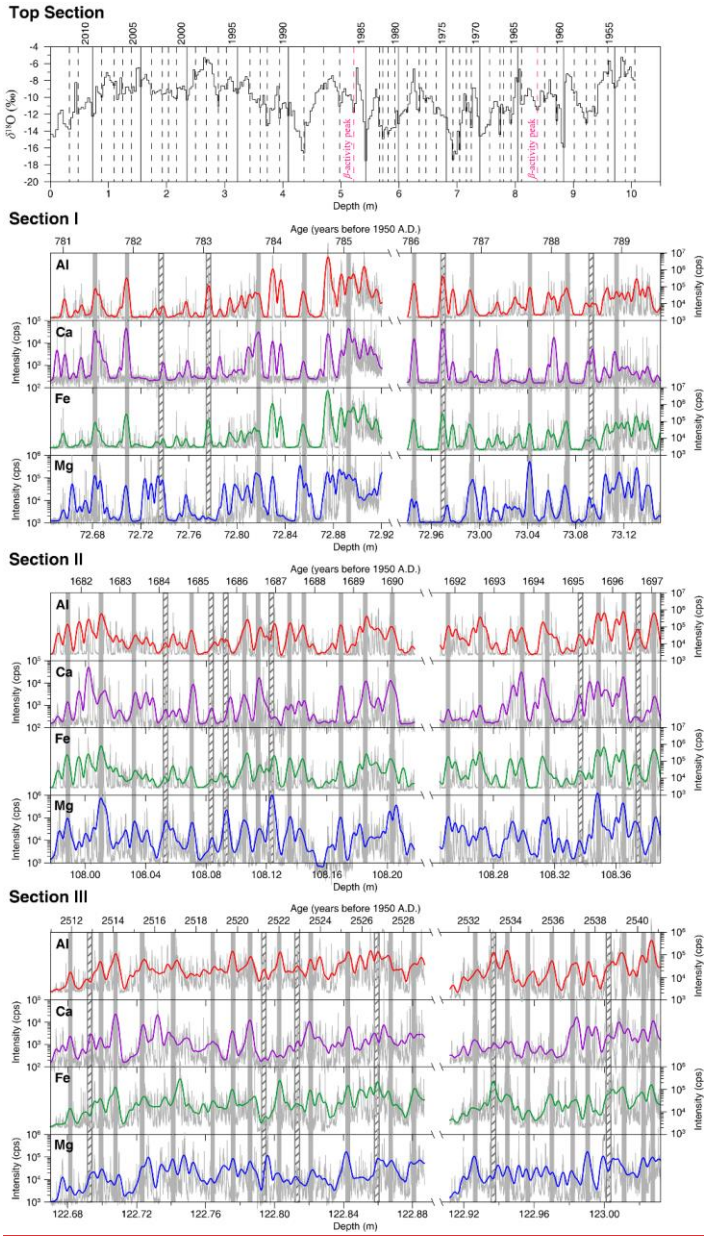

650 **Figure 2.** Annual layer counting for the Top Section, Section I, II, and III (top to bottom). The annual layers of the Top Section are identified based on the seasonality of $\delta^{18}O$ and two β-activity peaks (An et al., 2016). The annual layers of Section I, II, and III are marked at the winter/spring peaks (grey bars) of Al, Ca, Fe, and Mg concentrations. The open grey bars filled with forward slashes indicate uncertain

删除了: 1

annual layers. Thin grey lines indicate raw data, and thick colored lines represent 200-point Gaussian smoothing. LA-ICP-MS intensity is reported as counts per second.

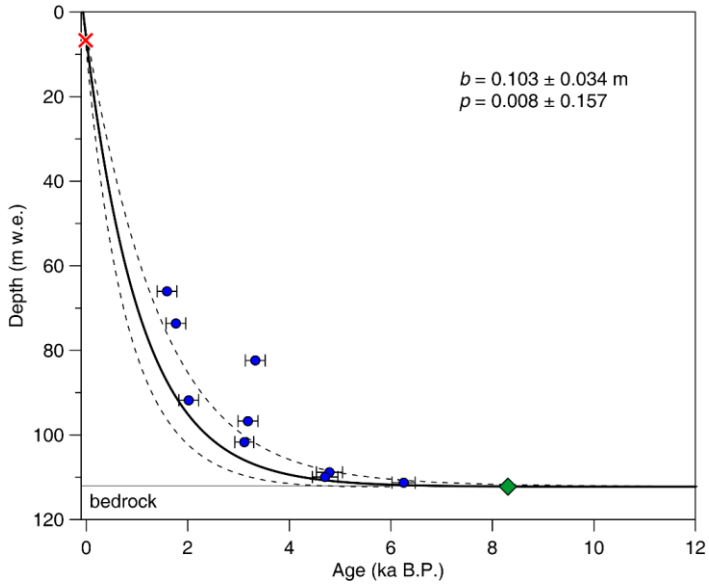

Figure 3. The depth-age relationship of the Chongce Core 2 based on the two-parameter model. The dashed lines represent the 1σ confidence interval of the two-parameter model fit (solid line). The red cross stands for the β activity peak in 1963 A.D., the blue dots the calibrated ^{14}C ages with 1σ error bar, green diamond for bedrock age estimate from the Chongce Core 4 (Hou et al., 2018; Zhang et al., 2018).

删除了: The annual layers of Section I, II, and III are marked at the winter/spring peaks (black dotted lines) of Al, Ca, Fe, and Mg concentrations. Thin grey lines indicate raw data, and thick colored lines represent 200-point Gaussian smoothing. LA-ICP-MS intensity is reported as counts per second.

删除了: 2

删除了:

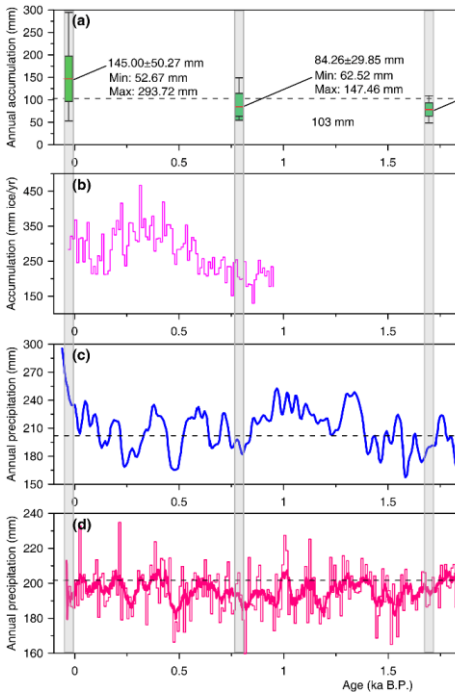

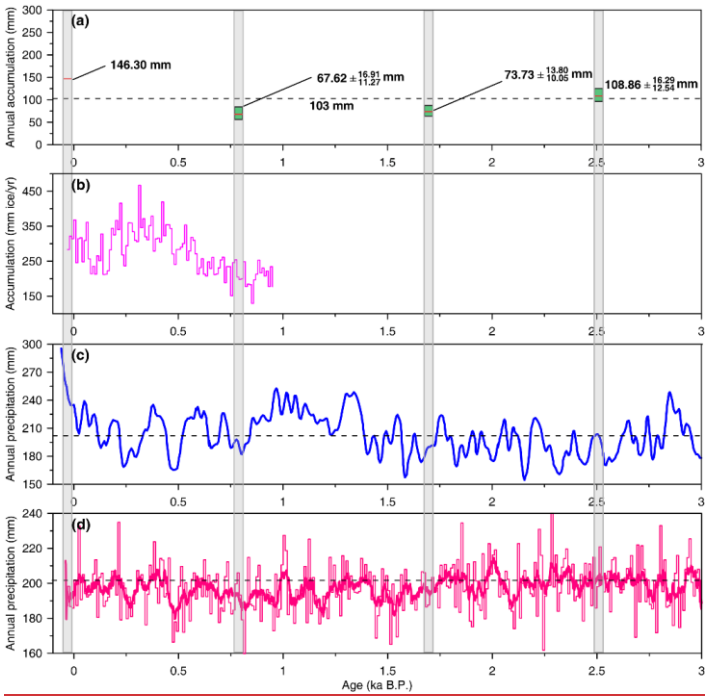

Figure 4. Our reconstructed annual accumulation for each of the four sections sampled (a) and its comparison with (b) snow accumulation reconstruction based on the Guliya ice core (Thompson et al., 2006), (c) precipitation reconstruction with 50-year smoothing in the northeastern TP (Yang et al., 2014), and (d) the TraCE-21 ka model results for the region (34-36°N, 80-82°E) (Collins et al., 2006). The dotted lines in (a) and (d) represent the average annual accumulation over the Holocene. The dotted line in (c) represent average annual accumulation over the past 3.0 ka. The thin and thick red lines in (d) represent 10-year and 50-year moving average respectively.

删除了: 3

Supplement of

A new method of resolving annual precipitation for the past millennia from Tibetan ice cores

Wangbin Zhang et al.

Correspondence to: Shugui Hou (shugui@nju.edu.cn; shuguihou@sjtu.edu.cn)

- **Text S1**
- Figures S1 to S7.
- Tables S1 to S2

删除了: 8

Text S1

In this study, the depth-age relationship of the Chongce 135.81 m Core 2 was established by using a two-parameter (2p) model. The 2p model was first constrained by the ^{14}C calibrated ages, together with the β-activity reference horizon of the Chongce 58.82 m Core 3, located only ~ 2 meters apart (Hou et al., 2018; Pang et al., 2020). We found that by using these data only, the 2p model is poorly constrained at the deep section, and giving an estimate bottom age much older than the bottom age ($8.3 \pm {}^{6.2}_{3.6}$ ka B.P.) estimated for Core 4 (Hou et al., 2018). Therefore, we included the Core 4 bottom age to constrain the final 2p model. Due to its mathematical configuration to account for ice flow dynamics, the 2p model gives more weight to points at shallower sections. Therefore, the inclusion of the Core 4 bottom age (relatively younger than otherwise derived bottom age) pushes the curve towards the left (younger) of most ^{14}C dates. However, we believe this model gives the most reasonable results, compared with several other model fit based on different data combinations (Fig. S7). The details of these model fits are provided as follows.

(1) all data (including β-activity peak of Core 3 and nine ^{14}C ages) (Fig. S7a).

Results: The derived annual accumulation rate of 137 ± 54 mm w.e./year is in good agreement with the value of 140 mm w.e./year based on the tritium horizon. But the model is poorly constrained in deeper sections: the derived age estimate at the depth of the deepest ^{14}C sample is $9.1 \pm {}^{7.2}_{4.0}$ ka B.P.. This is much older than the actual measured ^{14}C age of 6.3 ± 0.2 ka B.P. at that depth (Fig. S7a).

(2) all data (including β-activity peak of Core 3 and nine ^{14}C ages) and constant accumulation rate (140 m w.e./year) (Fig. S7b).

Results: The derived ice age at the bedrock is $30.7 \pm {}^{44.8}_{18.4}$ ka B.P., which is much older than the bottom age ($8.3 \pm {}^{6.2}_{3.6}$ ka B.P.) estimated for Core 4. In addition, the derived age estimate at the depth of the deepest ^{14}C sample is $9.2 \pm {}^{6.0}_{3.6}$ ka B.P.. This is much older than the ^{14}C age of 6.3 ± 0.2 ka B.P. at that depth. (Fig. S7b).

(3) β-activity peak of Core 3 and oldest six ^{14}C ages (Fig. S7c).

Results: The derived ice age at the bedrock is $22.5 \pm {}^{34.8}_{13.8}$ ka B.P., which is much older than the bottom age ($8.3 \pm {}^{6.2}_{3.6}$ ka B.P.) estimated for Core 4. In addition, the derived accumulation (233 ± 104 mm w.e./year) deviates significantly from the β-activity based estimate (140 mm w.e./year) (Fig. S7c).

(4) β-activity peak of Core 3, oldest six ^{14}C ages, and constant accumulation rate (140 mm w.e./year) (Fig. S7d).

Results: The derived ice age at the bedrock is $50.1 \pm \frac{118.4}{35.6}$ ka B.P., which is much older than the bottom age ($8.3 \pm \frac{6.2}{3.6}$ ka B.P.) estimated for Core 4. In addition, the derived age estimate at the depth of the deepest ^{14}C sample is $9.6 \pm \frac{7.3}{4.1}$ ka B.P.. This is much older than the ^{14}C age of 6.3 ± 0.2 ka B.P. at that depth (Fig. S7d).

(5) all data (including β-activity peak of Core 3 and nine ^{14}C ages) plus bedrock estimate from Core 4 (Hou et al., 2018) as an additional model input point (**the method used in this manuscript**) (Fig. S7e).

Results: The derived ice age at the bedrock is $9.0 \pm \frac{7.9}{3.6}$ ka B.P., which is roughly consistent with the bottom age ($8.3 \pm \frac{6.2}{3.6}$ ka B.P.) estimated for Core 4. The derived accumulation rate (103 ± 34 mm w.e./year) is in relative agreement with the β-activity based estimate (140 mm w.e./year). In addition, the modeled age at the depth of the deepest ^{14}C sample is now $5.2 \pm \frac{1.9}{1.2}$ ka B.P. which, with the uncertainty range, is similar to the ^{14}C age of 6.3 ± 0.2 ka B.P. (Fig. S7e). We believe this model provides most reasonable results, and is therefore adopted for this paper.

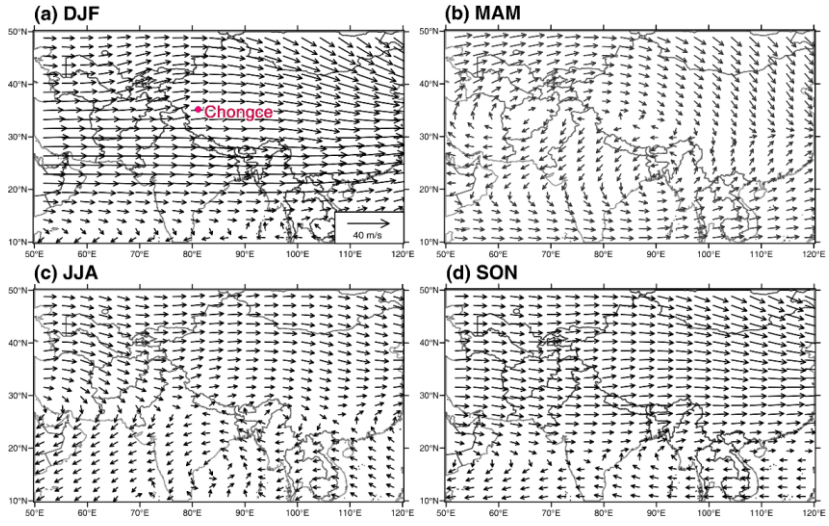

Figure S1. Seasonally averaged horizontal wind patterns at 500 hPa over the Tibetan Plateau and its vicinity. Wind speed data are from the ERA 5 (available at: https://www.ecmwf.int/).

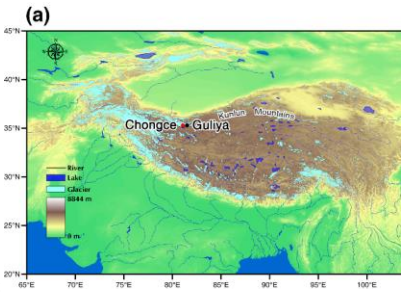

删除了:

Figure S1. (a) Map showing the drilling sites of Chongce (red solid dot) and Guliya ice cores (black solid dot). The topographic data were extracted from the ETOPO1 elevations global data, available from National Oceanic and Atmospheric Administration at http://www.ngdc.noaa.gov/mgg/global/global.html. (b) Remote sensing image showing Chongce ice cap and the locations of ice core drilling sites. Blue contour lines indicate ice thickness.

删除了: 2

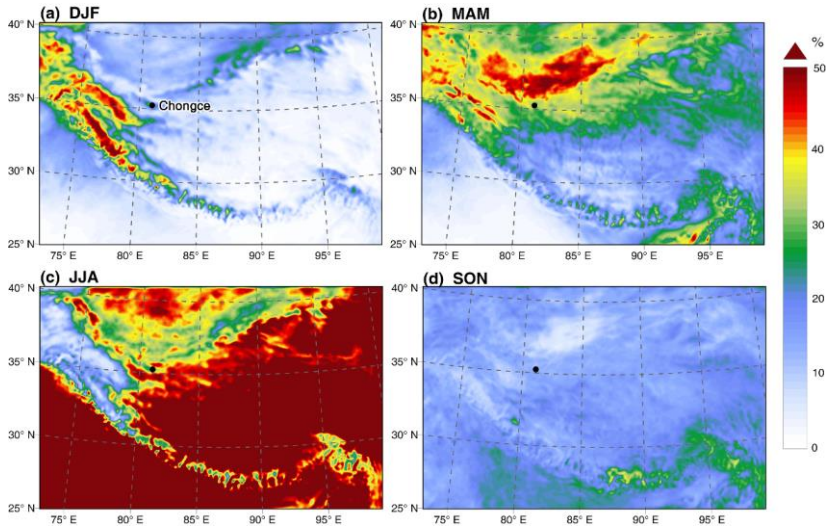

Figure S2. Seasonal precipitation regimes on the Tibetan Plateau. Percentage of annual precipitation in winter (DJF) (a), spring (MAM) (b), summer (JJA) (c), and fall (SON) (d), calculated by the High Asia Refined analysis dataset (2001-2013 AD) with spatial resolution of 10 km (Maussion et al., 2014).

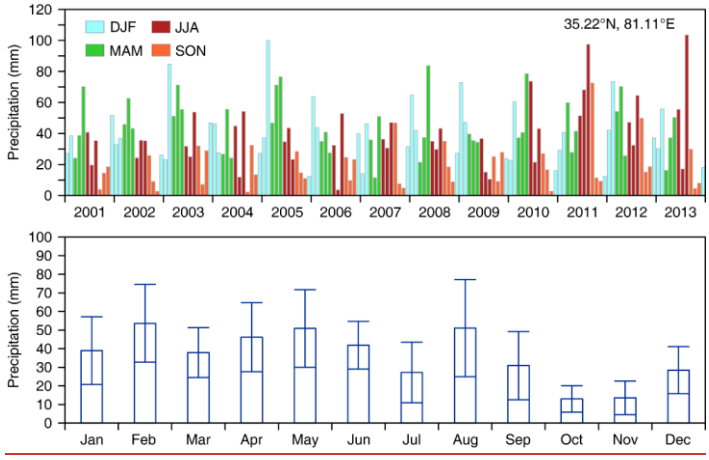

Figure S3. Monthly precipitation distribution in the vicinity of the Chongce ice cap, as shown by High Asia Refined monthly data from 2001 A.D. to 2013 A.D. (top) and by the monthly climatology for this period (bottom) (Maussion et al., 2014). Approximately 27.8% of annual precipitation falls from June to August, 13.3% from September to November, 27.9% from December to February, and 31.1% from March to May.

删除了: 3

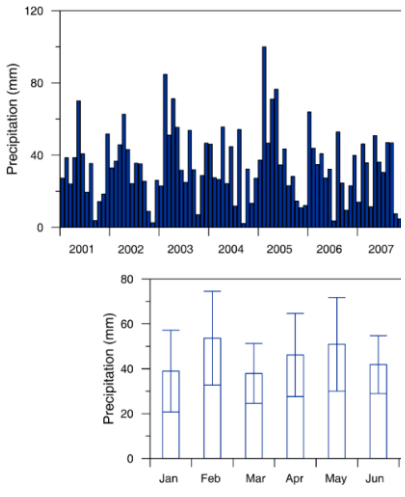

删除了:

删除了: 4

删除了: The seasonal

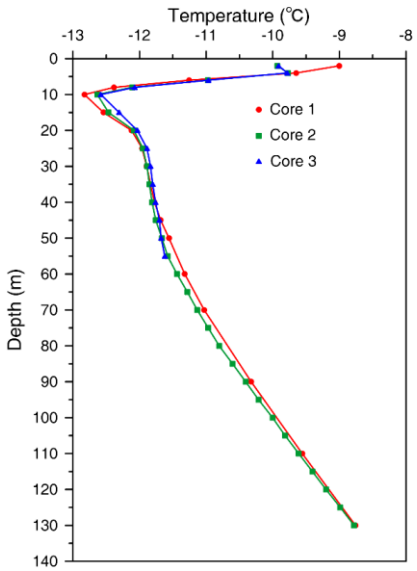

Figure S4: Borehole temperature profiles of the Chongce Core 1, Core 2 and Core 3

删除了: 5

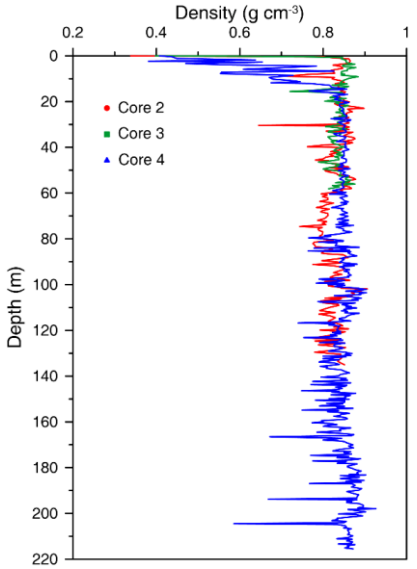

90

Figure S5. Density profiles of the Chongce Core 2, Core 3 and Core 4.

删除了: 6

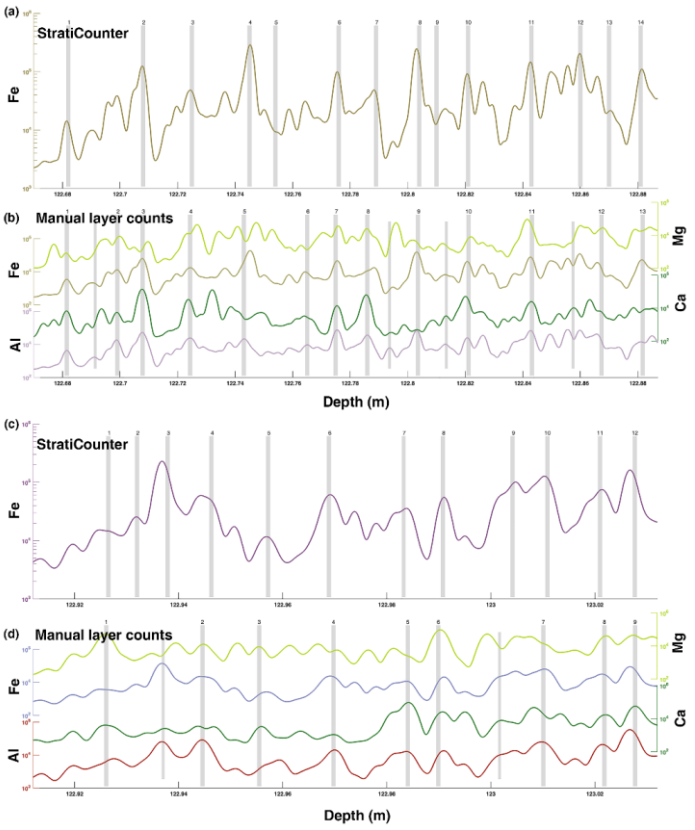

95

Figure S6. StratiCounter assignment of annual layers for Section III (a, c). Manual assignment of annual layers for Section III (b, d). The annual layers of Section III are marked at the winter/spring peaks (grey bars) of Al, Ca, Fe, and Mg concentrations. The short grey bars indicate uncertain annual layers.

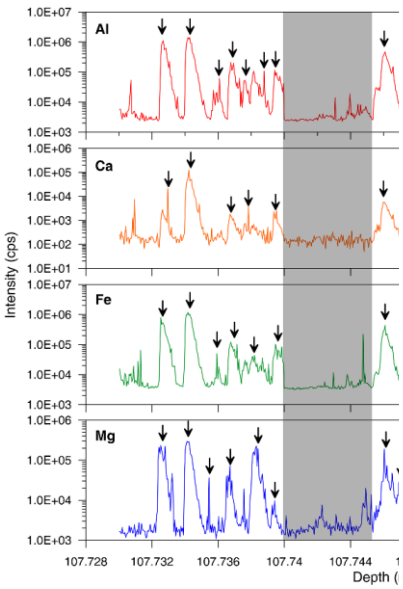

删除了:

Figure S7. Annual layer counting example taken from Section II, an ~4 cm section shown for Al (red), Ca (orange), Fe (green), and Mg (blue). Black arrows show multiple individual peaks, which can be considered as sub-annual dust events during winter and spring. Grey bars show 'synchronous' trough in all the four elements (Al, Ca, Fe, and Mg) measured, which can be considered as summer snow layers with weak dust deposition.

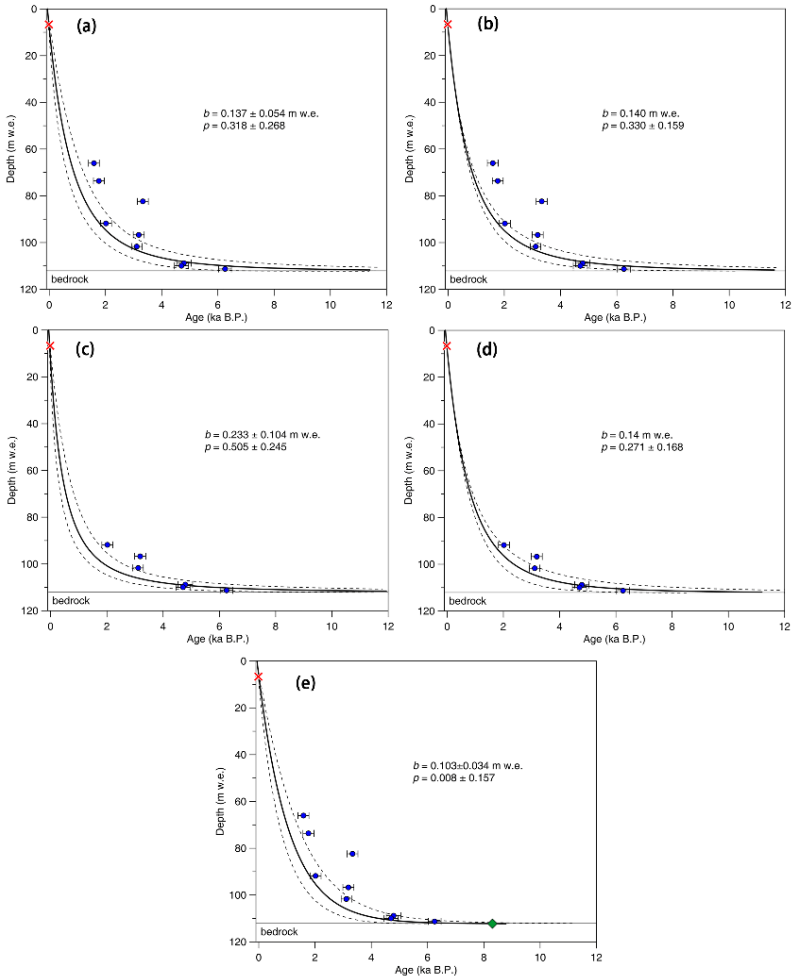

Figure S7. The depth-age relationship of the Chongce Core 2 based on the two-parameter model.

Table S1. Details of ice samples for β-activity measurements.

Sample #	Depth (m)	Depth (m w.e.)	Length (m)	Length (m w.e.)	β activity (dph kg^{-1})
1	0.000-0.710	0.000-0.406	0.710	0.406	555.1
2	0.710-1.150	0.406-0.771	0.440	0.365	936.5
3	1.150-1.720	0.771-1.253	0.570	0.482	597.9
4	1.720-2.185	1.253-1.648	0.465	0.395	499.2
5	2.185-2.575	1.648-1.981	0.390	0.333	505.6
6	2.575-2.945	1.981-2.297	0.370	0.316	539.1
7	2.945-3.355	2.297-2.648	0.410	0.351	416.7

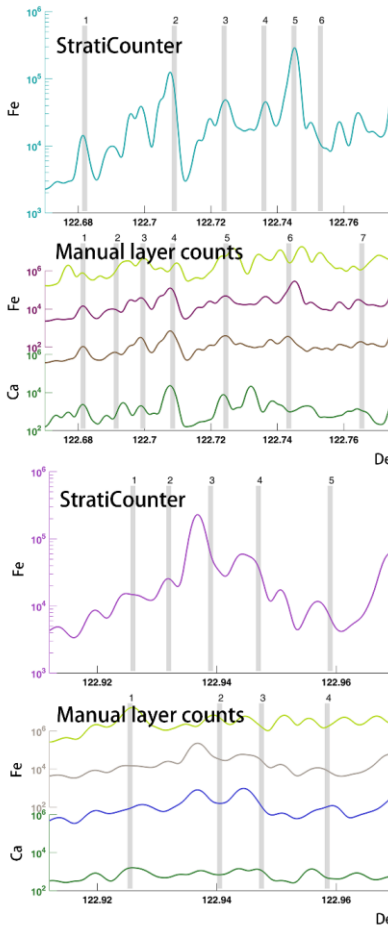

删除了:

Figure S8. Comparisons between StratiCounter and manual annual-layer counts (grey bars).

删除了: **Table S1.** The ^{14}C dating of 135.81 m Chongce ice core. Absolute uncertainties are given as 1σ range.

Sample #

8	3.355-3.890	2.648-3.110	0.535	0.462	518.4
9	3.890-4.350	3.110-3.504	0.460	0.393	396.1
10	4.350-4.805	3.504-3.889	0.455	0.385	439.4
11	4.805-5.270	3.889-4.288	0.465	0.399	1754.5
12	5.270-5.780	4.288-4.735	0.510	0.447	385.8
13	5.780-6.320	4.735-5.198	0.540	0.463	504.9
14	6.320-6.780	5.198-5.593	0.460	0.395	749.1
15	6.780-7.200	5.593-5.948	0.420	0.355	963.2
16	7.200-7.690	5.948-6.362	0.490	0.414	224.9
17	7.690-8.170	6.362-6.767	0.480	0.406	1709.9
18	8.170-8.630	6.767-7.158	0.460	0.390	1910.3
19	8.630-9.120	7.158-7.571	0.490	0.413	479.9
20	9.120-9.580	7.571-7.977	0.460	0.407	574.2
21	9.580-10.020	7.977-8.361	0.440	0.384	98.6
22	10.020-10.550	8.361-8.819	0.530	0.457	682.8
23	10.550-11.060	8.819-9.254	0.510	0.435	262.6
24	11.060-11.490	9.254-9.618	0.430	0.364	503.8
25	11.490-12.015	9.618-10.061	0.525	0.444	705.8
26	12.015-12.525	10.061-10.494	0.510	0.433	168.7
27	12.525-12.925	10.494-10.833	0.400	0.339	282.9
28	12.925-13.375	10.833-11.203	0.450	0.370	191.8
29	13.375-13.845	11.203-11.608	0.470	0.405	673.8
30	13.845-14.305	11.608-11.999	0.460	0.392	269.3
31	14.305-14.805	11.999-12.410	0.500	0.411	324.3

Table S2. Results of radiocabon measurements for the Chongce 135.81 m Core 2 ice core samples. For the calibrated calender year, ranges are given with 68.2% probalility.

Sample #	Depth (m)	Depth (m w.e.)	Mass (g)	WIOC (μg)	$F^{14}C$	^{14}C age (ka B.P.)[a]	calibrated age (ka B.P.)[b]
CC-1	79.46-80.21	65.74-66.31	307.7	20.3 ± 1.2	0.81 ± 0.01	1.679 ± 0.078	1.445-1.704
CC-2	88.82-89.56	73.31-73.92	302.9	24.3 ± 1.4	0.80 ± 0.01	1.831 ± 0.138	1.572-1.921
CC-3	99.44-100.10	82.12-82.65	304.6	13.8 ± 0.9	0.68 ± 0.01	3.133 ± 0.161	3.157-3.560
CC-4	110.58-111.35	91.48-92.10	342.6	24.9 ± 1.4	0.78 ± 0.01	2.037 ± 0.142	1.827-2.296
CC-5	116.62-117.43	96.39-97.05	330.9	9.1 ± 0.7	0.69 ± 0.01	3.012 ± 0.164	2.978-3.377
CC-6	122.64-123.36	101.40-101.98	338.6	17.6 ± 1.1	0.69 ± 0.01	2.944 ± 0.157	2.892-3.331
CC-7	131.41-132.10	108.54-109.12	324.6	22.6 ± 1.3	0.59 ± 0.01	4.228 ± 0.176	4.451-5.036
CC-8	132.65-133.51	109.59-110.31	392.7	23.6 ± 1.4	0.60 ± 0.01	4.169 ± 0.175	4.424-4.951
CC-9	134.31-135.03	110.98-111.59	292.4	23.0 ± 1.4	0.51 ± 0.01	5.466 ± 0.201	5.997-6.443

[a]"^{14}C age" denotes conventional radiocarbon age, which is calculated from the formula: $t = -8033 \times \ln(Fs)$, where t is conventional radiocarbon age, Fs is the ^{14}C / ^{12}C ratio of the sample divided by the same ratio of the modern standard.

[b]"calibrated age" denotes the calibrated age using OxCal v4.4 online program (Ramsey and Lee, 2013)

with the Northern (IntCal13) calibration curve (Reimer et al., 2013).